Fourier Monte Carlo Simulation of Hexatic Membranes

To cite this article: Andreas Tröster 2014 *J. Phys.: Conf. Ser.* **510** 012008

View the article online for updates and enhancements.

Related content

- Fourier Monte Carlo simulation of crystalline membranes in the flat phase
  Andreas Tröster

- Hexatic phase in two-dimensional Yukawa systems: Existence and properties
  X G Koss and O S Vaulina

- Tethering, Crumpling, and Melting Transitions in Hexatic Membranes
  E. Guitter and M. Kardar

Recent citations

- Fourier Monte Carlo renormalization-group approach to crystalline membranes
  A. Tröster

Fourier Monte Carlo Simulation of Hexatic Membranes

Andreas Tröster

Vienna University of Technology, Wiedner Hauptstrasse 8-10/136, A-1040 Wien, Austria

E-mail: `andreas.troester@tuwien.ac.at`

Abstract. Hexatic membranes are difficult to study both in theory as well as in simulations. We present new results for the flat phase of hexatic membranes using a unique simulation approach based on an recently developed optimization [1] of our Fourier Monte Carlo algorithm [2, 3] which enables us to drastically reduce critical slowing down and observe critical behavior with excellent statistical accuracy. In detail, we calculate the correlation function $\langle |\tilde{f}(\boldsymbol{q})|\rangle^2 = G(\boldsymbol{q})$ and the related mean squared displacement $\langle (\Delta f)^2 \rangle$ of the membrane's out-of-plane deformations in the Monge parametrization $f(\boldsymbol{x})$ and give a finite size scaling analysis of these data. In our present treatment, the case of hexatic membranes is formally found to closely resemble that of solid membranes for which our algorithm has already proven to be quite successful [1].

1. Introduction

The properties of membranes constitute an active research area of modern science. Membranes are ubiquitous in a biological context, they play an important role in advanced chemical synthesis and technology, and the research on graphene has recently been rewarded by a Nobel prize in physics for its exciting new perspectives on condensed matter physics and electronics. Motivated by the continuing interest in graphene, we have recently published high precision simulation data on the universal elastic fluctuation behavior of solid membranes.

Due to its strong covalent bondings, at low temperatures the properties of defect-free graphene come quite close to those of a "tethered membrane", i.e. a membrane model system whose bonds are by definition unbreakable. The caution implicit in this statement is based on the theoretical result that in reality there is nothing like a 2d "tethered" or "crystalline" membrane, since the Wagner-Mermin-Hohenberg theorem [4] assures us that in two dimensions true long-range translational order for systems with short-ranged interactions cannot exist. While the energy required to create an isolated dislocations in a strict 2d system grows logarithmically with system size, the energy of bound dislocations pairs in 2d turns out to be finite. Thus, at any low but positive T there is a nonzero density of such pairs. This implies that even at the lowest temperatures there is only quasi-long-range order in the density-density correlations, i.e. an algebraic decay with distance r exhibiting a T-dependent exponent. According to the Kosterlitz-Thouless-Halperin-Nelson (KTHNY) theory of 2d melting [5, 6, 7, 8, 9], above a certain critical temperature T_c the dislocation pairs break up, resulting in a gas of free dislocations and complete loss of translational order, but quasi-long-range *orientational* order of bonds persist in this *hexatic* phase. Free dislocations can, however, be in turn regarded as bound pairs

of orientational defects, so-called *disclinations* [10]. Below T_c the energy required to create an isolated disclination grows quadratically with system size, but once in the hexatic phase, the presence of free dislocations mediates a screening of this elastic energy that reduces this growth to a logarithmic one and thus facilitates the breaking-up of dislocation pairs at a still higher temperature T_m, resulting in complete destruction of the remaining orientational order. According to this KTNHY scenario, it is only above this second phase transition that the system assumes a true liquid state.

Membranes should, however, not be confused with true 2d systems in the above sense. Rather, they can be regarded as two-dimensional manifolds immersed in a 3d space, and whithin this embedding space they possess the additional freedom to bend and buckle, which allows them to drastically reduce the elastic energy required to create defect configurations. Even though taking into account the wave-vector dependent renormalization of the membrane's elastic constants considerably complicate the calculations, one can show [11] that for a membrane of size larger than a certain buckling radius R_b the energy of an isolated disclination is reduced from $\sim R_b$ to $\sim \ln R_b$, while that of a isolated dislocation decreases from $\sim \ln R_b$ to a finite constant. Thus, at arbitrary low but nonzero temperature there is always a finite concentration of free dislocations, and one concludes that any large enough would-be crystalline membrane is inevitably in a hexatic state, provided its size exceeds R_b.

Despite of these theoretical findings that guarantee the existence of hexatic membranes, it remains a challenge to study their properties, be it in experiment, theory or by computer simulation. In a real solid membrane like graphene, R_b may be prohibitively large, such that the hexatic nature of a specimen remains undetected in experiment and beyond reach in simulations based on microscopic or atomistic model Hamiltonians. In particular, this is true when it comes to precisely determining the universal long wavelength elastic properties of membranes, since for such simulations also large system sizes are required, and critical slowing down becomes a major obstacle. Thus, it comes as no surprise that the literature does not abound with computational studies of hexatic membranes [12]. In a recent paper [1] we have shown how to calculate the exponent η governing the asymptotic elastic behavior of solid membranes with great precision. The reason why this became possible was that we did not conduct simulations based on a "microscopic" Hamiltionian formulated on a lattice in direct space, but instead carried out Fourier Monte Carlo (FMC) simulations based on an effective Hamiltonian that focuses only on the long wavelength collective degrees of freedom. In addition, this algorithm also allows to efficiently suppress critical slowing down by performing an initial tuning step. It is the purpose of the present paper to extend this powerful approach to hexatic membranes in the low temperature flat phase.

2. Effective Hamiltonian

On the level of effective Hamiltonians, it turns out that even if their derivation proceeds quite differently in the solid and hexatic cases, the resulting expressions are extremely similar. In the so-called Monge parametrization of the low temperature flat phase, the "height" of a square membrane of projectted area $U = L \times L$ with coordinates $\boldsymbol{x} = (x_1, x_2) \in U$ is measured by a scalar function $f(\boldsymbol{x})$. Similar to the case of solid and liquid membranes, a hexatic membrane is subject to a harmonic bending energy

$$\mathcal{H}_{\text{hex}}^{(h)}[f] = \frac{\kappa_0}{2} \int_U d^2 x (\Delta f)^2(\boldsymbol{x}) \tag{1}$$

In addition, the hexatic membrane Hamiltonian has an anharmonic fourth order contribution of a structure that is formally quite similar to that for a solid membrane, although it originates from a rather different mechanism. Since the full derivation makes heavy use of differential geometry here we content ourselves with a quick sketch and refer the reader to the literature on

Riemannian manifolds (of which accessible accounts can be found e.g. in Refs. [13] or [14]) the original derivations [15, 16, 17] and the very nice reviews [18, 19] for further details.

The hexatic state is characterized by a unit vector field $\boldsymbol{n}(\boldsymbol{x})$ encoding the directional order of bonds, which, as we are targeting an underlying triangular lattice order, is defined only up to local 60° rotations. In writing down an effective continuum Hamiltionian, consider first such a field residing on a flat membrane. Then, the lowest order contribution would actually resemble a XY type of model, for which deviations from perfect parallelism of neighboring hexatic "directors" are subject to an energy penalty proportional to the squared gradient of $\boldsymbol{n}$. Introduction of (Gaussian) curvature leads, however, to a frustration of the field $\boldsymbol{n}(\boldsymbol{x})$, since the energetically most favorable parallel state cannot be maintained globally. Expressed in the Monge parametrization, the resulting coupling between the field $\boldsymbol{n}(\boldsymbol{x})$ and the Gaussian curvature of the membrane can be shown to be encoded in the anharmonic hexatic energy contribution

$$\mathcal{H}_{\text{hex}}^{(a)}[f,\theta] = \tag{2}$$
$$\frac{K_A}{2}\int_U d^2x \left(\partial_\mu \theta - \frac{1}{2}\epsilon_{\mu\sigma}\partial_\sigma \left[P_{\alpha\beta}^T (\partial_\alpha f)(\partial_\beta f)\right]\right)^2$$

where $P_{\alpha\beta}^T = \delta_{\alpha\beta} - \Delta^{-1}\partial_\alpha\partial_\beta$ is the so-called transverse projector (Δ^{-1} is, of course, the inverse Laplacian in 2d), $\theta = \theta(\boldsymbol{x})$ denotes the local bond angle (i.e. $\boldsymbol{n}(\boldsymbol{x}) = (\cos\theta(\boldsymbol{x}), \sin\theta(\boldsymbol{x}))$ with respect to a local orthonormal frame of the membrane's tangent bundle) and K_A is termed the hexatic stiffness.

In our present treatment, we assume that the field $\boldsymbol{n}(\boldsymbol{x})$ is single-valued and thus defect-free, which means that we neglect configurations with disclination defects. Thus, we expect to correctly describe the flat hexatic phase, but admittedly we will miss the disclination unbinding transition. The advantage of this assumption is, however, that it allows to completely eliminate the field $\boldsymbol{n}(\boldsymbol{x})$ from the partition function by virtue of a Gaussian integration. Up to an unimportant constant, one then obtains

$$\mathcal{H}_{\text{hex}}^{(a)}[f] = \frac{K_A}{2}\int_U d^2x \left(\frac{1}{2}\partial_\sigma P_{\alpha\beta}^T(\partial_\alpha f)(\partial_\beta f)\right)^2 \tag{3}$$

Comparing this expression to the corresponding anharmonic contribution for solid membranes (see Eqn. (2.14) of Ref. [20]), we note a close formal correspondence. In fact, the harmonic contributions are identical in structure, while the anharmonic contributions only differ because of the extra derivatives ∂_σ appearing in (3). Now recall [1] that in the solid case, we had been able to recast the anharmonic part of the membrane's effective Hamiltonian in a form

$$\mathcal{H}_{\text{sol}}^{(a)}[f] = \frac{K_0}{8}\int \frac{d^2Q}{(2\pi)^2}|\tilde{\mathcal{F}}_{\text{sol}}(\boldsymbol{Q})|^2 \tag{4}$$

that is diagonal in Fourier space, albeit not with respect to the amplitudes $\tilde{f}(\boldsymbol{q})$, but with respect to the generalized convolution amplitude

$$\tilde{\mathcal{F}}_{\text{sol}}(\boldsymbol{Q}) = \int \frac{d^2q}{(2\pi)^2}(\hat{\boldsymbol{Q}}\times\boldsymbol{q})^2 \tilde{f}(\boldsymbol{q})\tilde{f}(\boldsymbol{Q}-\boldsymbol{q}) \tag{5}$$

(K_0 denoted the solid membrane's 2d Young's modulus). Upon one partial integration in (3), the extra derivatives ∂_σ appearing in the present hexatic case translate into an extra squared

wave vector $\boldsymbol{Q}^2 = |\boldsymbol{Q}| \cdot |\boldsymbol{Q}|$ that can be equally distributed between the two $\mathcal{F}$-factors. Thus we finally end up with an effective Hamiltonian

$$\mathcal{H}_\Lambda[f] = \frac{\kappa_\Lambda}{2} \int \frac{d^2q}{(2\pi)^2} q^4 |\tilde{f}(\boldsymbol{q})|^2 + \frac{K_\Lambda}{8} \int \frac{d^2Q}{(2\pi)^2} |\tilde{\mathcal{F}}(\boldsymbol{Q})|^2 \tag{6}$$

for the hexatic system that looks exactly like that for a solid one, except that the amplitude

$$\tilde{\mathcal{F}}(\boldsymbol{Q}) := \int \frac{d^2q}{(2\pi)^2} |\boldsymbol{Q}| (\hat{\boldsymbol{Q}} \times \boldsymbol{q})^2 \tilde{f}(\boldsymbol{q}) \tilde{f}(\boldsymbol{Q} - \boldsymbol{q}) \tag{7}$$

inherits an extra factor $|\boldsymbol{Q}|$ in comparison to version (5) appropriate for solids. Note that in these last two formulas (6) and (7) we have dropped the explicit reference to the hexatic case, but have explicitly indicated a dependence of the coupling parameters on the presence of a wavevector cutoff Λ. Similar to the case of crystalline membranes, the anharmonic contribution to $\mathcal{H}_\Lambda[f]$ is again of a non-local nature, encoding an effective long-range anharmonic effective self-interaction of the field $f(\boldsymbol{x})$ mediated by the hexatic director field $\boldsymbol{n}(\boldsymbol{x})$ that effectively stiffens up the membrane at long wavelengths and thus stabilizes a low temperature flat phase.

3. Fourier Monte Carlo Approach

Criticality in systems with long-ranged interactions is very difficult to assess in a conventional Monte Carlo simulation based on a spins model defined on the direct lattice. In addition, the fact that the above model is formulated in terms of Fourier amplitudes rather suggests to employ our FMC algorithm [2, 3] which is tailor-made for such a situation. In a FMC simulation the continuous Fourier transform is replaced by a discrete Fourier transformation, for which we shall use the convention

$$f(\boldsymbol{x}) = \frac{1}{N} \sum_{\boldsymbol{q}} \tilde{f}(\boldsymbol{q}) e^{i\boldsymbol{q}\boldsymbol{x}}, \quad \tilde{f}(\boldsymbol{q}) = \sum_{\boldsymbol{x}} f(\boldsymbol{x}) e^{-i\boldsymbol{q}\boldsymbol{x}} \tag{8}$$

For periodic boundary conditions the admissible wave vectors $\boldsymbol{q}$ have components $|q_i| < \Lambda \leq \pi$ parametrized by integers $m_i \in \mathbb{Z}$ as $q_i = 2\pi m_i/L$, where we have put the lattice constant a of the underlying simple cubic lattice of $L^d = N$ sites to $a = 1$. A FMC move consists of picking a wave vector $\boldsymbol{q}_0$ and a complex number $\epsilon \in \mathbb{C}$ with $|\epsilon| \leq r$ at random, where $r > 0$ is some prescribed radius of a circle in the complex plane around zero. One then shifts

$$\tilde{f}(\boldsymbol{q}_0) \to \tilde{f}(\boldsymbol{q}_0) + \epsilon, \quad \tilde{f}(-\boldsymbol{q}_0) \to \tilde{f}(-\boldsymbol{q}_0) + \epsilon^*,$$

For the harmonic part $1/(2N) \sum_{|\boldsymbol{q}| \leq \Lambda} \kappa(\boldsymbol{q}) \tilde{f}(\boldsymbol{q}) \tilde{f}(-\boldsymbol{q})$ of a spin model Hamiltonian given in terms of the amplitudes $\tilde{f}(\boldsymbol{q})$, the accompanying energy change is easy to compute. The hard part is to calculate the change in the anharmonic part of the Hamiltonian in an efficient way. Since we have already reviewed the nuts and bolts of FMC in several publications [21, 22, 23], here we content ourselves with the following general statements.

FMC is certainly far from being a universal weapon for performing general simulation tasks in statistical mechanics. Rather than that, it has more of a specialized surgical tool that is capable of solving certain types of problems that had remained difficult to assess with other methods (see e.g. [2, 3]). In particular, FMC is a powerful strategy for studying critical behavior in systems with effective or microscopic long-range, since the Fourier transform diagonalizes all interactions irrespectively of their range as long as they are translationally invariant [24], and the move scheme (8) is nonlocal and collective. Of course, the algorithm becomes only efficient to use if a rather small cutoff Λ enclosing the critical wave vector, which is usually $\boldsymbol{q}_c = \boldsymbol{0}$, is chosen,

and all "fast" models outside the cutoff are regarded as having been integrated out from the partition function, such their effect is absorbed in the remaining effective "Landau-Ginzburg" Hamiltonian governing the behavior of the "slow modes" $\tilde{f}(\boldsymbol{q})$ with $|\boldsymbol{q}| < \Lambda$. In an application to crystalline membranes, it was recently even demonstrated [1] that by slightly modifying the above scheme one may obtain an algorithm that is practically free of critical slowing down in the sense that at criticality the integrated autocorrelation times of the amplitudes $\tilde{f}(\boldsymbol{q})$ show only negligible growth when approaching $\boldsymbol{q} \to \boldsymbol{0}$. This major improvement that catapults FMC into the top league of algorithms for studying criticality in interactions with long range is achieved by simply allowing for different values $r(\boldsymbol{q})$ for the radius r governing the maximum change in amplitude in the MC move (8), and optimizing these radii $r(\boldsymbol{q})$ separately for, say, $30 - 40\%$ acceptance rates during the start-up of the simulation. A further advantage of FMC is that it is parallelizeable using standard MPI and OpenMP approaches.

4. Results and Discussion
Similar to the approach used in Ref. [1], we have calculated the out-of-plane displacement correlation function

$$\tilde{G}(\boldsymbol{q}) = \langle |\tilde{f}(\boldsymbol{q})|^2 \rangle \tag{9}$$

and the related out-of-plane mean squared displacement

$$\langle (\Delta f)^2 \rangle = \int \frac{d^2 q}{(2\pi)^2} G(\boldsymbol{q}) \tag{10}$$

for the effective Hamiltonian (6). The largest system accessible to our available computer resources at a wave vector cutoff $\Lambda = \pi/8$ had a linear size $L = 1096$ (thus effectively corresponding to a real space system of linear size $8 \times 1096 = 8552$), and for finite size scaling we used the sequence $L = 296, 329, 360, \ldots, 1096$ of system sizes at the same cutoff. Our choice of parameters $\kappa_\Lambda = 1.0$ and $K_\Lambda = 10.0$ was motivated by the desire to have an approximate balance between harmonic and anharmonic energy contributions in the simulation. In Fig. 1 we present the results for $G(\boldsymbol{q})$ in a double logarithmic plot. We recall that for a solid membrane one expects $G^{-1}(\boldsymbol{q}) \sim \kappa(\boldsymbol{q})q^4$, with a renormalized $\boldsymbol{q}$-dependent bending stiffness $\kappa(\boldsymbol{q}) \sim q^{-\eta}$ that shows an infra-red power law divergence with a critical exponent η that characterizes the nontrivial critical elastic behavior of the membrane [1]. For the hexatic case at hand, however, we report that the best fit to the data was obtained for a scaling ansatz

$$\tilde{G}(\boldsymbol{q}) \sim \frac{k_B T}{\kappa_R(q)q^4}, \qquad \kappa_R(q) = \kappa_0 + \gamma \ln \frac{\delta}{q} \tag{11}$$

of logarithmic type rather than a "true" power law (κ_0, γ and δ denote fit parameters). In other words, our present findings would thus suggest a value $\eta = 0_{\log}$. However, our precision is hampered by the finite size of the system and the lack of a concrete crossover ansatz capturing the crossover from mean field to critical behavior for $\boldsymbol{q} \to 0$. Thus, a small nonzero value of the exponent η cannot be ruled out. As to $(\Delta f)^2$, such a logarithmic behavior is compatible with a finite size scaling ansatz of type

$$(\Delta f)^2 \sim \omega + \alpha^2 L^2 (1 + \beta \log L + \rho/L)$$

with parameters $\omega, \alpha, \beta, \rho$. Indeed, a corresponding fit of our data for $(\Delta f)^2$ shown in Fig. 2 seems to support this reasoning. Unfortunately it is not straightforward to compare our results to analytical predictions for the exponent η. In Ref. [16], a field-theoretic renormalization group
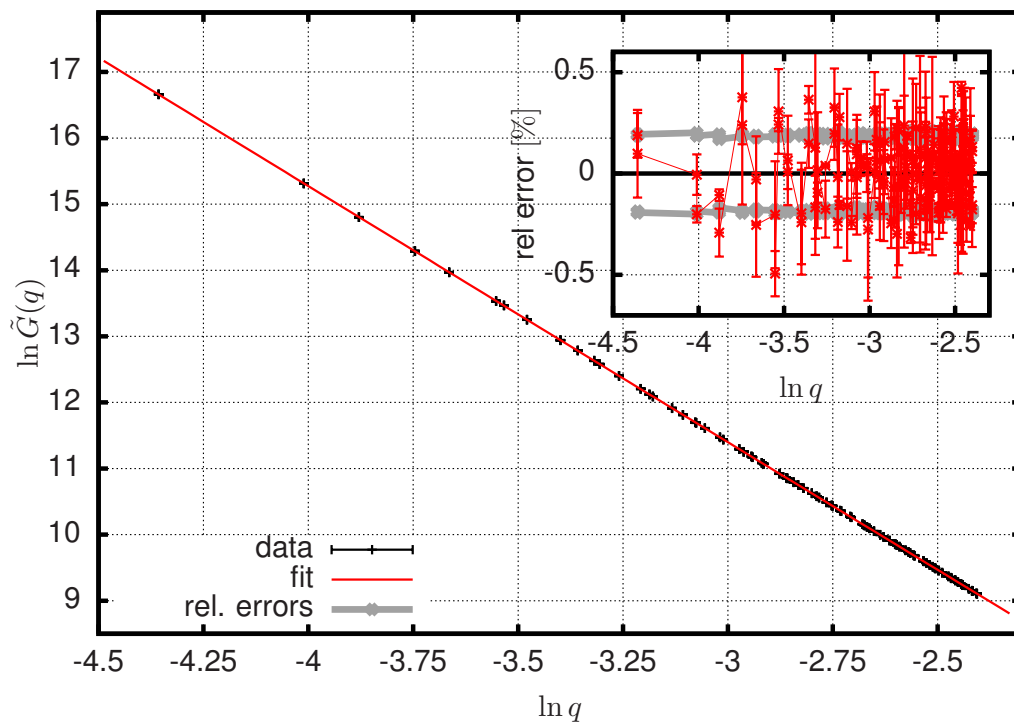
Figure 1. Top: fit of simulation results for $G(\boldsymbol{q})$ at linear system size $L = 1096$ and cutoff $\Lambda = \pi/8$. Error bars are smaller than symbol size. Bottom: Relative deviations of simulation data from the fit. Red lines are a guide to the eye. Gray lines indicate the relative statistical errors of the simulation data in percent.

(RG) analysis based on expansions in inverse powers of K_Λ was worked out to first order in $1/K_\Lambda$, and a line of fixed points with a value η continuously depending on the parameter K_Λ is found. For the corresponding exponent η that describes this so-called *crinkled phase*, the result

$$\eta = O(1/K_\Lambda^2) \tag{12}$$

was obtained, which obviously is compatible with our above findings. However, as recently shown by Codello and Zanusso [25] using the machinery of the exact RG, η is not only nonzero to second order in $1/K_\Lambda$, but moreover also receives contributions from the fixed point value μ_Λ^* of the (bare) *surface tension* coefficient μ_Λ to this order. To the accuracy of the Monge parametrization, the contribution of out-of-plane fluctuations $\tilde{f}(\boldsymbol{q})$ on the surface tension is captured by the term

$$\mathcal{H}_\Lambda^{(s)} = \mu_\Lambda \int \frac{d^2 q}{(2\pi)^2} q^2 |\tilde{f}(\boldsymbol{q})|^2 \tag{13}$$

and near the crinkled phase fixed point $(\kappa_\Lambda^*, \mu_\Lambda^*)$, the parameter μ_Λ represents a *relevant* coupling. Thus, to obtain an accuracy beyond $O(1/K_\Lambda)$ for the exponent η, it is necessary to consider the energy (13) in addition to the membrane Hamiltonian (6). Furthermore, in order to reach the crinkled phase fixed point, the bare surface tension parameter μ_Λ must be tuned such as to be located on the critical manifold $\mathcal{C}$ of the crinkled phase fixed point, which represents a line in the projected renormalization flow plane with coordinates $(\kappa_\Lambda, \mu_\Lambda)$. Thus, even though
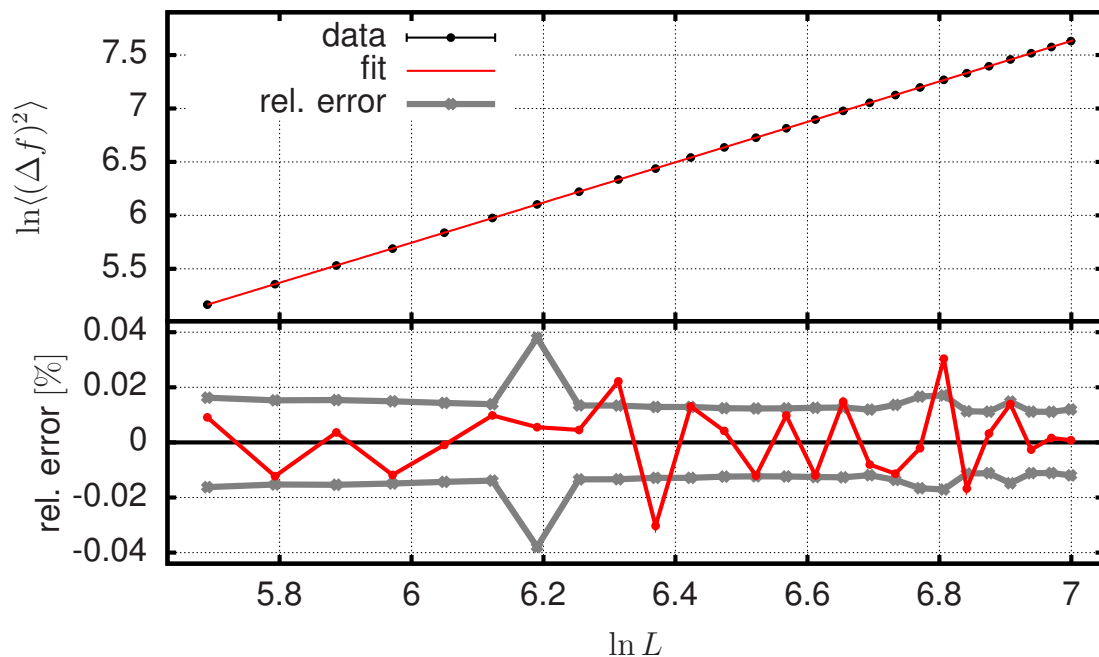
Figure 2. Top: fit of FSS ansatz (12) to simulation results for $\langle(\Delta f)^2\rangle$ obtained for $L = 296, 329, 360, \ldots, 1096$ and $\Lambda = \pi/8$. Error bars are smaller than symbol size. Bottom: Relative deviations of simulation data from the fit. Red lines are a guide to the eye. Gray lines indicate the relative statistical errors of the simulation data in percent.

the slope of this line in the $(\kappa_\Lambda, \mu_\Lambda)$-plane may not be steep, it may well be that our above numerical efforts, which are aimed at describing the critical behavior of the crinkled phase, have actually been contaminated from an (hopefully small) accumulated nonzero value for μ_Λ picked up during integrating out the implicit integration of modes in the FMC simulation.

Since the Hamiltonian (13) is also harmonic, it is principle straightforward to incorporate it into our simulations. The trouble is, however, that it is difficult to actually make sure that the system at hand was indeed critical. That is, for constant K_Λ and a given a fixed value κ_Λ, one must find an accurate calculation scheme for determining the specific value $\mu_\Lambda^{(c)} = \mu_\Lambda^{(c)}(\kappa_\Lambda, K_\Lambda)$ of the bare surface tension μ_Λ such that the point $(\kappa_\Lambda, \mu_\Lambda^{(c)})$ is located on the critical manifold $\mathcal{C}$. For the moment, ignoring this difficulty by putting $\mu_\Lambda \equiv 0$ was all we could do. This problem is, however, not specific to our present approach. Rather than that, any simulation approach that attempts to study the crinkled phase is challenged by this difficulty. Yet, in contrast to other simulation strategies, FMC also offers a way out of this difficulty, as FMC in principle also allows to implement a momentum shell RG scheme from which the RG flow of the parameters κ_Λ, μ_t can actually be calculated [26]. Knowledge of this flow then makes it possible to assess the desired crinkled fixed point and determine its critical manifold $\mathcal{C}$. As shown in Refs. [27, 28], such a RG scheme does not merely represent a qualitative description of what is going on, but can be further optimized to even produce decent quantitative numerical results. While beyond the scope of the present paper, work in this direction is currently in progress.

References

[1] Tröster A 2013 *Phys. Rev. B* **87**(10) 104112 URL http://link.aps.org/doi/10.1103/PhysRevB.87.104112
[2] Tröster A 2007 *Phys. Rev. B* **76** 012402
[3] Tröster A 2008 *Phys. Rev. Lett.* **100** 140602
[4] Mermin N and Wagner H 1966 *Phys. Rev. Lett.* **17** 1133
[5] Kosterlitz J M and Thouless D J 1973 *Journal of Physics C: Solid State Physics* **6** 1181
[6] Coleman S 1973 *Communications in Mathematical Physics* **31** 259–264 ISSN 0010-3616 URL http://dx.doi.org/10.1007/BF01646487
[7] Young A P 1979 *Phys. Rev. B* **19**(4) 1855–1866 URL http://link.aps.org/doi/10.1103/PhysRevB.19.1855
[8] Halperin B and Nelson D R 1978 *Phys. Rev. Lett.* **41** 121
[9] Nelson D R and Halperin B I 1979 *Phys. Rev. B* **19**(5) 2457–2484 URL http://link.aps.org/doi/10.1103/PhysRevB.19.2457
[10] Nelson D R 2002 *Defects and Geometry in Condensed Matter Physics* (Cambridge, UK: Cambridge University Press)
[11] Carraro C and Nelson D R 1993 *Phys. Rev. E* **48**(4) 3082–3090 URL http://link.aps.org/doi/10.1103/PhysRevE.48.3082
[12] Gompper G and Kroll D M 1997 *Phys. Rev. Lett.* **78**(14) 2859–2862 URL http://link.aps.org/doi/10.1103/PhysRevLett.78.2859
[13] Carroll S M 2004 *Spacetime and Geometry: An Introduction to General Relativity* (San Francisco: Addison Wesley)
[14] Frankel T 2012 *The Geometry of Physics* 3rd ed (New York: Cambridge University Press)
[15] Nelson D and Peliti L 1987 *J. Phys. (Paris)* **48** 1085
[16] David F, Guitter E and Peliti L 1987 *J. Physique* **48** 2059
[17] Nelson D, Piran T and Weinberg S (eds) 2004 *Statistical Mechanics of Membranes and Surfaces, Second Edition* (Singapore: World Scientific)
[18] Bowick M J and Travesset A 2001 *Physics Reports* **344** 255 – 308 ISSN 0370-1573 URL http://www.sciencedirect.com/science/article/pii/S0370157300001289
[19] Bowick M J and Giomi L 2009 *Advances in Physics* **58** 449–563 (*Preprint* http://www.tandfonline.com/doi/pdf/10.1080/00018730903043166) URL http://www.tandfonline.com/doi/abs/10.1080/00018730903043166
[20] Nelson D 2004 *Statistical Mechanics of Membranes and Surfaces, Second Edition* (Singapore: World Scientific) chap 6. Theory of the Crumpling Transition, p 131
[21] Tröster A and Dellago C 2007 *Ferroelectrics* **354** 225
[22] Tröster A and Dellago C 2010 *Physics Procedia* **6** 106 – 116 ISSN 1875-3892 URL http://www.sciencedirect.com/science/article/pii/S1875389210006504
[23] Tröster A 2008 *Comput. Phys. Commun.* **179** 30–33
[24] Tröster A 2010 *Phys. Rev. B* **81** 012406
[25] Codello A and Zanusso O 2013 *Phys. Rev. E* **88**(2) 022135 URL http://link.aps.org/doi/10.1103/PhysRevE.88.022135
[26] Tröster A 2009 *Phys. Rev. E* **79** 036707
[27] Tröster A 2010 *Phys. Rev. B* **81** 125135
[28] Tröster A 2011 *Comput. Phys. Commun.* **182** 1837 – 1841 ISSN 0010-4655 URL http://www.sciencedirect.com/science/article/pii/S0010465510004510